INT. J. REMOTE SENSING, 2002, VOL. 23, NO. 24, 5177–5192

Taylor & Francis
Taylor & Francis Group

Satellite remote sensing of land surface temperatures: application of the atmospheric correction method and split-window technique to data of ARM-SGP site

S. C. OU, Y. CHEN, K. N. LIOU

Department of Atmospheric Sciences, 7127 Math Sciences Building, University of California, 405 Hilgard Avenue, Los Angeles, CA 90095-1565, USA; e-mail: ssou@atmos.ucla.edu

M. COSH and W. BRUTSAERT

School of Civil and Environmental Engineering, Cornell University, Hollister Hall, Ithaca, NY 14853-3501, USA

(*Received 6 April 2001; in final form 27 September 2001*)

Abstract. The performance of algorithms for the satellite remote sensing of land surface temperatures based on an atmospheric correction method and a split-window technique was examined. For this purpose, we employed comprehensive data collected over the Atmospheric Radiation Measurement Program (ARM) Southern Great Plain (SGP) Cloud and Radiation Testbed (CART) site for a number of manually determined clear and mostly clear dates during 1997 and 1999 with cloud coverage of less than 10%. The data sources included brightness temperature data measured by the Advanced Very High Resolution Radiometer (AVHRR) on-board National Oceanic and Atmospheric Administration (NOAA)-12 and NOAA-14, collocated and coincident observed surface temperatures derived from the solar and IR radiation observing system (SIROS) and solar and IR station (SIRS) data, and balloon-borne atmospheric sounding profiles. For the application of the atmospheric correction method, we used the Moderate Resolution Transmittance Model (MODTRAN) 3.7 to compute transmittances and atmospheric radiances. In the present study, comparison of the retrieved surface temperatures with observations obtained at the central and external facility sites over the SGP area shows that the accuracy of the atmospheric correction scheme is closer to the requirement that is acceptable for estimating surface latent heat fluxes than the split-window method.

1. Introduction

Numerous algorithms for the remote sensing of land surface temperature (LST) have been developed using data collected by space-borne imaging sensors, including the Advanced Very High Resolution Radiometer (AVHRR) on-board the National Oceanic and Atmospheric Administration (NOAA) polar-orbiters and the thermal infrared (IR) imagers on-board the Geostationary Operational Environmental Satellite (GOES) satellites. Retrievals using these algorithms have illustrated that it is possible to obtain realistic and reasonable LST distributions over large geographical regions. Satellite-derived LST can be assimilated to climate, mesoscale and land–atmosphere coupling models to estimate components of the surface energy balance. In particular, Brutsaert *et al.* (1993) used surface temperatures derived from measurements by the AVHRR 10.9

International Journal of Remote Sensing
ISSN 0143-1161 print/ISSN 1366-5901 online
http://www.tandf.co.uk/journals
DOI: 10.1080/01431160110115050

and 12.0 μm channels on-board the NOAA-9 satellite in conjunction with collocated temperature and wind soundings in the boundary layer to determine surface sensible and latent heat fluxes from forests in south-west France. The authors concluded that it is important to achieve high accuracy ($\sim$0.5 K) in the satellite-retrieved LST in order to reduce the uncertainty in the estimated surface latent heat fluxes.

Two types of retrieval method have been developed to estimate LST from space: the atmospheric correction method and the split-window technique. The atmospheric correction method requires the support of an accurate radiative transfer model together with atmospheric temperature and humidity profiles as input. These profiles must be determined from conventional radiosonde data or satellite soundings. The accuracy of removing atmospheric absorption/emission effects is subject to errors in radiative transfer model calculations, and uncertainties in atmospheric gaseous (predominantly water vapour) absorption coefficients, and input atmospheric temperature, humidity and trace gas profiles. To quantify the atmospheric radiative transfer, a series of atmospheric transmittance/radiance codes with varying spectral resolutions and progressively detailed compilations of atmospheric absorption line/band parameters (HITRAN series) has been developed in the past two decades and widely applied to the development of satellite remote sensing algorithms for retrieving LST and other atmospheric and surface parameters. These codes include the Low Resolution Transmission Model (LOWTRAN)-5, -6 and -7 (Kneizys *et al.* 1983, 1988), and the Moderate Resolution Transmission Model (MODTRAN) (Berk *et al.* 1989). In particular, MODTRAN 3.7 uses a multiple scattering approximation to account for aerosol scattering and absorption, and gaseous absorption is considered based on band models. The split-window technique connects atmospheric and surface emissivity effects based on the differential absorption characteristics of a pair of split-window channels (Becker and Li 1990, Wan and Dozier 1996). This type of algorithm, though simple and fast, is expected to be less accurate than the atmospheric correction technique.

Satellite-based LST measurements have not been used operationally in regional weather and climate prediction because of large uncertainties in the retrieval algorithms. The accuracy of most of the satellite LST retrievals is limited to the reliability of the removal of water vapour absorption/emission effects. The current satellite split-window LST algorithm performs retrievals on spatial scales of $\sim$8 km with 1–4 K measurement uncertainties (Becker and Li 1990, Dozier and Wan 1994, Prata 1994, Coll and Caselles 1997). Becker and Li (1995) stated that the satellite LST retrieval can achieve an accuracy of 1 K, but several assumptions about the surface state, aerosol effects, and atmospheric properties are required. On the other hand, the atmospheric correction method has the potential of achieving an accuracy of $\sim$0.5 K in LST retrievals. However, since radiative transfer calculations require substantial computer resources, its application to large-scale and global mapping of LST requires further improvement and development.

The objective of this paper is to investigate the performance of the preceding two types of LST retrieval algorithms, and to validate the two retrieved LSTs with collocated and coincident surface observations. For this purpose, we take advantage of the established data collection system over the Atmospheric Radiation Measurement Program (ARM-SGP) Cloud and Radiation Testbed (CART) site, and acquire a mosaic of AVHRR data, ground-based surface temperature measurements, and balloon-borne atmospheric sounding profiles. We use MODTRAN 3.7 to compute atmospheric transmittances and radiances for manually determined clear and mostly clear dates with a cloud coverage of less than 10%. The organization of this paper is as follows. Section 2 presents the

fundamentals of the two LST retrieval programs. Data sources and results of the retrievals are described in §3 and 4, respectively. Finally, conclusions are given in §5.

2. Methodologies for satellite retrieval of land surface temperatures

The atmospheric correction method is based on atmospheric radiative transfer calculations (e.g. Brutsaert *et al.* 1993). From the formal solution of the fundamental radiative transfer equation (e.g. equation (2.1.10a) of Liou 1992 with modification), the upward radiance at the top of atmosphere is given by

$$I_v^+(z_\infty,\mu)=\left[\varepsilon_v B_v(0)+(1-\varepsilon_v)\int_{z=0}^{z=z_\infty} B_v(z)\frac{d[T_v(z,z_\infty)]}{dz}dz\right]T_v(0,z_\infty)$$
$$+\int_{z=z_\infty}^{z=0} B_v(z)\frac{d[T_v(0,z)]}{dz}dz \qquad (1)$$

where ε_v is the surface emissivity at wavelength v, $B_v(0)$ is the Planck function of wavelength v for the surface temperature ($z=0$), $T_v(0,z_\infty)$ is the transmittance between the surface and the top of atmosphere ($z=z_\infty$), $B_v(z)$ is the Planck function for the temperature associated with height z, and $T_v(0,z)$ is the transmittance between the surface and height z. In equation (1), the first term represents the contribution from the surface emission and reflection of downward atmospheric emission that is attenuated by the entire vertical column of the atmosphere, while the second term denotes the contribution from the atmospheric emission characterized by the Planck intensity multiplied by the weighting function $d[T_v(0,z)]/dz$.

For the work reported here, we will assume $\varepsilon_v=1$ for the following reasons. The surface emissivity for typical natural soil and vegetation and for the spectral interval 10–12 μm varies between 0.95 and 0.99 (Sutherland 1986). We have performed synthetic retrievals to study the effects of surface emissivity based on MODTRAN-generated 10.9 and 12 μm radiances for a range of precipitable water between 0 and 4 g cm^{-2}. Results show that differences of the retrieved surface temperatures based on $\varepsilon_v=1$ and 0.95 are of the order of 0.1 K, about 0.03% of mean retrieved LST. For desert areas, the emissivity effect on the retrieved surface temperature will be more significant due to lower surface emissivity values. Since the land surface types over the ARM-SGP CART site are mostly grazed vegetation and range land, we expect the assumption $\varepsilon_v=1$ would not incur significant error for the surface temperature retrievals. To simulate the upward radiance measured by a satellite sensor, I_{sat}, we may perform integration of both sides of equation (1) over the satellite sensor's band width, weighted by the channel response function, $\phi(v)$, to obtain

$$I_{sat}=I_{sfc}\,\Im+I_{atm}^{\uparrow} \qquad (2)$$

where

$$I_{sat}=\int I_v^+(z_\infty,\mu)\phi(v)dv$$

$$I_{sfc}=B_{\bar{v}}(0)$$

$$\Im=\int T_v(0,z_\infty)\phi(v)dv$$

$$I_{atm}^{\uparrow}=\int\phi(v)dv\int_{z=z_\infty}^{z=0} B_v(z)\frac{d[T_v(0,z)]}{dz}dz$$

The term I_{sat} can be computed from satellite measurements, while $\Im$ and $I^{\uparrow}_{atm}$ can be evaluated from the atmospheric profiles of temperature and humidity. It follows that I_{sfc} and subsequently the surface temperature can be derived from equation (2).

In the present study, we used the MODTRAN 3.7 radiance model (Berk *et al.* 1989) to compute $\Im$ and $I^{\uparrow}_{atm}$ for AVHRR 10.9 μm (ch. 4) and 12 μm (ch. 5) channels. The balloon-borne sounding profiles for temperature and humidity were used as inputs to the MODTRAN 3.7. To determine the retrieved temperature from equation (2), it would be ideal to have the values of $\Im$ and $I^{\uparrow}_{atm}$ based on the sounding for each pixel. However, this is not practical because the soundings are launched only at specific surface meteorology sites. For this reason, we compute $\Im$ and $I^{\uparrow}_{atm}$ based on soundings at a 'central facility' site and apply them to the whole retrieval domain. Moreover, these sounding profiles normally were not coincident with the satellite overpass. For the cases where the satellite passage did not coincide with the sounding, we compute $\Im$ and $I^{\uparrow}_{atm}$ for soundings just prior to and after the passage. The corrected radiance, I_{sfc}, at the time of the satellite passage was then obtained using linearly interpolated $\Im$ and $I^{\uparrow}_{atm}$ between the values associated with the two soundings. Finally, the retrieved surface temperature is obtained as the average of those derived from chs 4 and 5 I_{sfc}.

In the split-window technique, the difference in brightness temperatures of the AVHRR ch. 4 and ch. 5 was used to correct the temperature value in ch. 4. A variety of formulations of the split-window technique has been developed. However, these expressions can be generalized into the following form:

$$T_{sfc} = a + bT_4 + cT_5 \tag{3}$$

where coefficients a, b and c are dependent on both the surface emissivity and the atmospheric properties (Coll and Caselles 1997). For the same localized domain, as in the current case, these coefficients are obtained from retrieved surface temperatures from the atmospheric correction method. The resulting coefficient values can be treated as corresponding to a domain-averaged surface emissivity and mean atmospheric state. It is clear that this method is much more efficient than the atmospheric correction method, but its accuracy is limited.

3. Data sources

In order to compare the performance of the two LST retrieval algorithms, we employ the comprehensive data collected over the ARM-SGP CART site, which was established to fulfil the data requirements of the ARM Science Team. This site covers the Southern Kansas and Northern Oklahoma regions, located within a rectangular box from 34.5–38.5° N latitude and from 95–100° W longitude. Among potential test sites within the continental United States, the SGP-CART land surface is relatively homogeneous. It is primarily composed of wheat fields, pastures, native prairie and grazed and ungrazed rangeland. Moreover, its topography shows that the local terrain within the site is generally simple, ranging from very flat land surface to mildly rolling hills. These characteristics are conducive to obtaining high quality surface measurement data and are essential for carrying out validation of the retrieved surface temperatures. The data collection began in the early 1990s, and the data archiving started in 1993. For the present study we utilized inputs derived from the satellite data, ground-based radiometric measurements, and balloon-borne atmospheric soundings.

AVHRR satellite images taken over the ARM SGP-CART site are based on the

reflected solar and emitted thermal infrared (IR) radiances observed by the AVHRR on-board NOAA satellites. The raw data were downlinked to the Sea Space receiving station in San Diego, and subsequently processed at the Pacific Northwest National Laboratories. They were finally archived at the Oak Ridge National Laboratory. These images were rectified to a Mercator projection, centered at the SGP Central Facility (CF; 36.605° N, 97.485° W), which is near Lamont, Oklahoma. The domain of each image consists of 500 rows of data, and each row consists of 350 pixels, with a pixel resolution of about 1 km. A matching overlay file containing the latitude and longitude for each pixel was also obtained and applied to find the geographical coordinates of selected measurement sites.

The files include calibrated radiance fields as well as the brightness temperatures for the thermal IR channels. Brightness temperatures are stored as short integers in units of 0.1° C, and radiances as short integers in units of 0.01 $\mathrm{mW\,m^{-2}\,sr^{-1}\,cm}$. The visible channel (chs 1 and 2) image data are in albedo units that were calibrated using the pre-launch channel characteristics as distributed by NOAA. Data for the solar and satellite zenith angles and sun–satellite azimuthal angles are also included. The files are in hierarchy data format (hdf; generated by TeraScan by the tdftohdf routine). The images were taken from the closest-to-overhead pass of the afternoon and morning satellites. NOAA-14 overpasses were at about 0140 and 1340 local standard time, with $\sim \pm 1$ h variations determined by the orbit, while NOAA-12 overpasses were at about 0730 and 1930 local standard time, with $\sim \pm 1$ h variations.

Various ground-based instruments were deployed near the CF and 24 extended facility (EF) sites. The EF sites were scattered within the SGP-CART site box. Until the end of 1997, the solar and IR radiation observing system (SIROS) was deployed at CF and many of the EF sites. The SIROS was composed of pyranometers (ventilated and shielded), pyrgeometers (ventilated and shielded), a normal incidence pyrheliometer on a solar tracker, and the multi-filter rotating shadowband radiometer (MFRSR). These radiometers measured upwelling and downwelling solar and IR irradiances. For the purpose of validating the retrieved LST, we used the upwelling long-wave hemispheric irradiance measured by the downward-looking pyrgeometers for selected clear or mostly clear dates within 1997. The SIROS went offline toward the end of 1997. Starting in late 1998, a new system called the solar and IR station (SIRS), which replaced the SIROS, was installed. This new system has an improved solar and IR radiometric observing system data-logging capability. The broadband radiometric instruments of SIRS are virtually the same as those of SIROS. The SIRS pyrgeometers are the Eppley Laboratory's Precision Infrared Radiometers (PIR). This instrument measures separately downward and upward thermal IR radiative fluxes at the surface. Its spectral response curve ranges approximately from 3.5–50 μm. New data loggers and the associated data collection equipment were installed to provide an independent data-logging system for those broadband radiometer instruments only, while the MFRSR, which was previously a part of SIROS, now has a separate data-logging system. Thus, the SIRS platform can achieve considerably greater stability and reliability of the measured radiometric data than the previous SIROS system. Again, for the validation of the retrieved LST, we used the upwelling long-wave hemispheric irradiance measurements for selected clear or mostly clear dates in 1999.

In addition, for the purpose of computing the atmospheric emission and transmission terms in equation (1) using MODTRAN 3.7, sounding profiles were required. The temperature and humidity data were obtained from the balloon-borne sounding

system (BBSS). Generally, the BBSS was launched every 3 h each day. Before 1997, the routine radiosonde launch times at the central facility were chosen to facilitate the Instant Radiative Flux (IRF) and Instrument Development Program (IDP) research. After 1998, however, the new routine radiosonde launch times at the CF were chosen to complement the National Weather Service standard launch times of 0000 and 1200 UTC, and at the same time to support the daytime satellite (mainly NOAA/AVHRR) overpass at approximately 2030 UTC.

4. Results and discussion

We applied the atmospheric correction and split-window algorithms to the AVHRR data collected over the ARM-SGP CART site and analysed a total of 34 satellite overpass scenes. They are divided into two groups according to the year that they were collected. Tables 1 and 2 give the dates and NOAA satellite overpass times as well as the meteorological sounding launch times at CF for these scenes. There were 12 scenes taken from the 1997 data archive, as shown in table 1. Six of them were during the winter (January–February), while the rest were during the following autumn (September–October). Also, five scenes corresponded to NOAA-14 overpasses and seven scenes were associated with NOAA-12 overpasses. Table 2 lists 22 scenes taken from the 1999 data archive, within summer–autumn (August–October), all of which were associated with NOAA-14 overpasses. Based on manual

Table 1. Collocated NOAA satellite overpass and sounding times for 1997 cases. Also listed are the computed AVHRR 10.9 μm and 12 μm transmittances and atmospheric radiances based on the sounding profiles at the ARM-SGP CART Central Facility site for each satellite overpass.

Date (MMDD)	Sounding time (HHMM UTC)	Overpass time (HHMMSS UTC)	Transmittance		Atmospheric radiance (W m^{-2} sr^{-1} cm)	
			T_v (10.9 μm)	T_v (12 μm)	$I^{\uparrow}_{atm}$ (10.9 μm)	$I^{\uparrow}_{atm}$ (12 μm)
6 January	1130	090839 (14)	0.946	0.923	0.244E-02	0.551E-02
6 January	2033	203112 (14)	0.949	0.929	0.224E-02	0.520E-02
17 January	0529 1129	084951 (14)	0.949	0.930	0.177E-02	0.363E-02
17 January	1731 2034	201217 (14)	0.951	0.933	0.238E-02	0.526E-02
28 January	1730 2029	195401(14)	0.964	0.961	0.147E-02	0.289E-02
1 February	0529	135741 (12)	0.873	0.806	0.919E-02	0.180E-01
29 September	2324 0526	003922 (12)	0.867	0.791	0.113E-01	0.227E-01
29 September	1127 1427	130042 (12)	0.876	0.811	0.103E-01	0.202E-01
30 September	2326 0224	001802 (12)	0.849	0.772	0.131E-01	0.249E-01
2 October	1124 1424	133318 (12)	0.684	0.555	0.290E-01	0.488E-01
5 October	2326 0228	000910 (12)	0.651	0.517	0.324E-01	0.533E-01
6 October	1130 1425	134518 (12)	0.627	0.491	0.345E-01	0.561E-01

Table 2. Collocated NOAA satellite overpass and sounding times for 1999 cases. Also listed are the computed AVHRR 10.9 μm and 12 μm transmittances and atmospheric radiances based on the sounding profiles at the ARM-SGP CART Central Facility site for each satellite overpass.

Date (MMDD)	Sounding time (HHMM UTC)	Overpass time (HHMMSS UTC)	Transmittance		Atmospheric radiance ($W\,m^{-2}\,sr^{-1}\,cm$)	
			T_v (10.9 μm)	T_v (12 μm)	$I^{\uparrow}_{atm}$ (10.9 μm)	$I^{\uparrow}_{atm}$ (12 μm)
11 August	0530 1129	103117 (14)	0.538	0.389	0.447E-01	0.687E-01
11 August	2037 2329	215306 (14)	0.629	0.491	0.363E-01	0.588E-01
12 August	0529 1131	102024 (14)	0.666	0.534	0.329E-01	0.541E-01
12 August	2031 2328	214219 (14)	0.572	0.427	0.425E-01	0.666E-01
13 August	0530 1131	100908 (14)	0.753	0.642	0.230E-01	0.402E-01
13 August	2037 2338	213127 (14)	0.724	0.605	0.250E-01	0.431E-01
18 August	0532 1131	105203 (14)	0.737	0.620	0.227E-01	0.393E-01
18 August	2030 2332	221409 (14)	0.738	0.623	0.250E-01	0.433E-01
19 August	0531 1130	104105 (14)	0.714	0.594	0.264E-01	0.448E-01
19 August	2030 2232	220303 (14)	0.852	0.778	0.136E-01	0.262E-01
22 September	0531 1131	105835 (14)	0.887	0.831	0.842E-02	0.166E-01
22 September	2029 2330	222035 (14)	0.878	0.816	0.980E-02	0.194E-01
5 October	0834 1133	101326 (14)	0.829	0.747	0.137E-01	0.256E-01
5 October	2029 2329	213534 (14)	0.846	0.769	0.131E-01	0.252E-01
6 October	0831 1128	100245 (14)	0.773	0.672	0.200E-01	0.356E-01
6 October	2031 2330	212446 (14)	0.755	0.650	0.219E-01	0.390E-01
12 October	0830 1134	103410 (14)	0.784	0.683	0.198E-01	0.355E-01
12 October	2031 2330	215555 (14)	0.809	0.717	0.176E-01	0.326E-01
13 October	0531 1136	102304 (14)	0.810	0.717	0.170E-01	0.311E-01
13 October	2030 2331	214512 (14)	0.851	0.774	0.122E-01	0.236E-01
14 October	0831 1133	101213 (14)	0.831	0.746	0.140E-01	0.263E-01
14 October	2034 2331	213416 (14)	0.852	0.776	0.133E-01	0.257E-01

examination, all of the scene images indicate that the SGP site was under either clear or mostly clear sky, with cloud coverage of less than 10% of the total area. Transmittances and atmospheric radiances for the two thermal IR window channels were obtained for each sounding listed in tables 1 and 2. For the cases with two soundings available (one before and one after the satellite overpass), we obtain the transmittances and atmospheric radiances corresponding to the satellite overpass by interpolation of transmittances and atmospheric radiances associated with the respective soundings. Differences in the transmittances and atmospheric radiances for soundings of 3-h and 6-h time intervals are negligibly small for those winter cases of 1997. This implies that values for the two parameters are nearly constant for the dry and cold atmosphere in winter. Therefore, for 6 January (two cases) and 1 February (one case) 1997, with only one sounding available for each case, the transmittances and atmospheric radiances corresponding to the sounding time were directly applied to the retrievals. The transmittances for winter cases are generally larger than those for the summer cases due to less water vapour. Atmospheric radiances are generally smaller in winter than in summer due to colder atmospheric temperature.

To apply the split-window technique, we used the retrieval results from applying the atmospheric correction method to the 1997 data. It was our intention to employ certain established split-window methods with emissivity-dependent coefficients. However, because of the limited amount of data in the present study, and the uncertainty of the AVHRR chs 4 and 5 surface emissivity for the type of surfaces within the ARM-SGP domain, we chose to use a multidimensional least-square fit method. We apply this method to the 94 cases of the retrieved surface temperatures at selected EF sites based on the atmospheric correction method versus the satellite measured brightness temperatures of chs 4 and 5. We obtained the value for the coefficients in equation (3): $a=-7.409$, $b=1.251$ and $c=-0.217$. These coefficients were then applied to the 1999 data to obtain the surface temperatures based on the split-window technique.

For the purpose of presentation and discussion, we first illustrate the comparison of geographically mapped retrieved surface temperatures from the atmospheric correction and split-window techniques based on a single case. Subsequently, we present validation of the retrieved LST for the 1997 and 1999 cases against the SIROS and SIRS data, respectively. Finally, we discuss the spatial and temporal characteristics of errors in the retrieved LST.

4.1. *Geographical distribution of retrieved LST for 1023 UTC, 13 October 1999*

To illustrate the comparison between the two LST retrieval algorithms, the scene of 1023 UTC 13 October 1999, was selected as an example. This date falls within the period of the Cooperative Atmosphere-Surface Exchange Study (1999). The weather synopsis for this date showed that a weak surface front moved through the area overnight. Surface winds were south-easterly, beginning light but becoming stronger as the day progressed. At the time of the NOAA-14 overpass (1023 UTC), corresponding to the early morning of 13 October at the ARM site, AVHRR images showed that the area was almost completely cloudless.

Figure 1 displays the images of 10.9 μm brightness temperature, the LSTs retrieved based on the split-window and atmospheric correction algorithms, and the LST difference determined from the two algorithms. Overlapped with figure 1(*a*) are the locations of the 22 EF sites. The various dark spots in the image are associated with

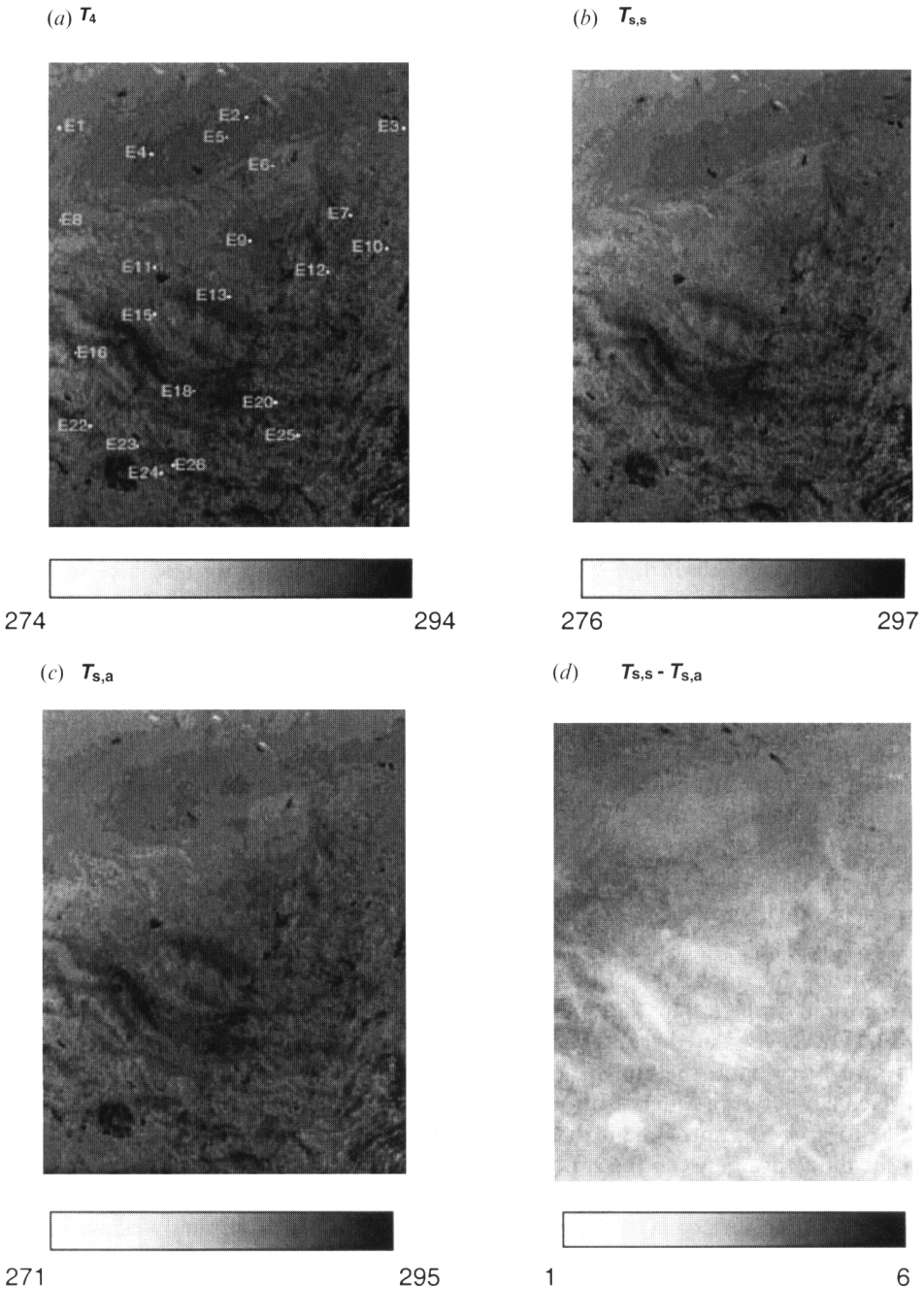

Figure 1. Display of (*a*) AVHRR 10.9 μm brightness temperature overlapped with the location of 22 EF sites; (*b*) the retrieved LSTs from the split-window method; (*c*) the retrieved LSTs from the atmospheric correction method; and (*d*) the difference in retrieved LSTs from the split-window and atmospheric correction methods, over a $4.5^\circ \times 5^\circ$ area around the ARM-SGP CART site on 13 October 1999. The NOAA-14 overpass time is 1023 UTC. The coordinates of the four corners of the image are: north-west; 38.81541° N, 99.43618° W; north-east; 38.81786° N, 95.53033° W; south-west; 34.32882° N, 99.44079° W; and south-east; 34.33261° N, 95.53484° W.

lake and river water surfaces, since the brightness temperature over these water surfaces is generally higher than that over land. The distribution of the 10.9 μm brightness temperature is evidently following terrain features. The shape of curving rivers and the change of land surface types are vaguely displayed.

Referring to figures 1(*b*) and (*c*), the patterns of the retrieved LSTs are grossly similar to those of the 10.9 μm brightness temperatures. The retrieved LSTs range from 276–297 K using the split-window algorithm, and from 271–295 K employing the atmospheric correction algorithm. Both soundings at 0531 UTC (local nighttime) and 1136 UTC (local early morning) show that there is a near-surface temperature inversion. Thus, some of the retrieved LSTs by the atmospheric correction method are lower than the corresponding ch. 4 brightness temperatures. The retrieved LSTs by the split-window technique, on the other hand, failed to reflect the near-surface inversion effects. Both algorithms produce higher LSTs over the southern region. The distribution of LST differences produced by the two algorithms, as shown in figure 1(*d*), reveals that the average LST retrieved from the split-window technique is higher than that from the atmospheric correction algorithm by about 3 K. This average difference could be caused by uncertainty in the correction of the water vapour effects using the brightness temperature differences of the two thermal IR window channels in the split-window algorithm. The terrain and lake features that are evident in figure 1(*a*)–(*c*) are less distinct in figure 1(*d*). Generally, the difference over the warmer surfaces associated with water, relatively more humid areas and urban regions (Wichita in the north and Oklahoma City in the south), is smaller than that over the colder surfaces associated with northern land surfaces, because the coefficients of the split-window method are determined based on the statistical fitting of retrieved temperatures, which are on average warmer than the average temperature over dry land surfaces for the present case.

4.2. *Validations using the SIROS and SIRS data*

To validate the retrieved LSTs, we used the surface temperature measurements derived from the SIROS data for the EF sites whose locations are depicted in figure 1(*a*). The surface temperature values were obtained from downward-looking radiometer measurements. Effects of water vapour emission/absorption between the ground surface and radiometer were corrected based on parametrizations of MODTRAN simulated radiative fluxes as described below. We denote the measured upward broadband thermal IR radiative flux as F, and assume that the observed surface temperature differs from the equivalent black-body temperature by a factor of ε. To a good approximation, this factor can be assumed to be a linear function of the difference between the surface ($T_{s,obs}$) and air temperatures (T_a). Furthermore, the coefficients of this linear function may be expressed in terms of a quadratic function of the surface layer water vapour mixing ratio, q. After analyses, we have

$$T_{s,obs} = \frac{(F/\sigma)^{1/4} - A + BT_a}{1+B} \tag{4}$$

where σ is the Stefan-Boltzmann Constant, and A and B are coefficients which are functions of q in the forms

$$A = a_1 + b_1 q + c_1 q^2 \tag{5}$$

$$B = a_2 + b_2 q + c_2 q^2 \tag{6}$$

where a_i, b_i and c_i are empirical coefficients. To determine these coefficients, we have acquired a set of 8344 atmospheric sounding profiles ($\Delta p = 25$ mb) taken by TOVS (the NOAA-88 file for the development of the next-generation temperature retrieval algorithm and other purposes). Profiles that were within the domain of the SGP site were selected and applied to MODTRAN 3.7 and F at 10 m above ground were computed for three prescribed surface temperatures: $T_a - 6$, T_a, $T_a + 6$. The coefficients were then obtained by linear (equation (4)) and quadratic (equations (5) and (6)) least square fitting methods. Their values are: $a_1 = -0.0061$, $b_1 = 2.5035$, $c_1 = -124.86$, $a_2 = 0.1163$, $b_2 = 14.195$ and $c_2 = -306.43$. Error analyses indicate this method of correction is highly accurate with errors in the corrected surface temperature due to fitting no more than 0.04 K. Once these coefficients were determined, we applied them to compute the surface temperatures from the SIROS and SIRS data based on equations (4)–(6). The magnitude of correction, that is, the difference between the corrected and equivalent black-body temperatures, varies between 0–3 K. Higher humidity and larger surface-air temperature jump lead to larger magnitude of correction.

Figure 2 shows the time series of the radiometer temperatures for eight EF sites on 30 September 1997. The weather synopsis for this date was similar to that for 13 October 1999. There was a weak front passing through the site overnight. The upper air was dominated by a high pressure dome, as shown in the 300, 500 and 700 mb height charts. The vertical air column was relatively dry, as indicated by a low relative humidity of less than 60%. This diagram contains information regarding both the spatial and temporal variation in the retrieved LSTs. The temporal variation pattern of the temperature for all eight sites is similar. Starting from 0000 UTC (local sunset), the temperature continues to decrease until around 1200 UTC (local sunrise), at which point it reaches a minimum value. With the solar radiation

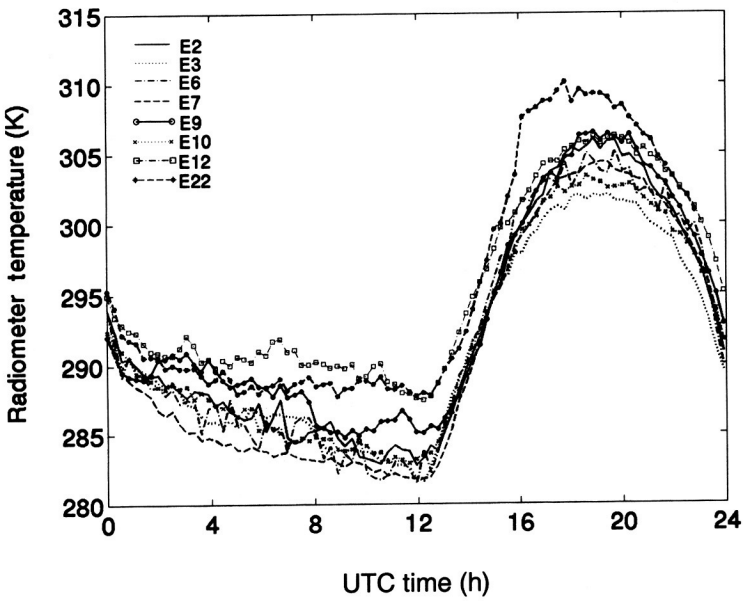

Figure 2. The time series of the ARM-SGP surface radiometric temperatures derived from the SIROS data at eight sites whose locations are depicted in figure 1(*a*) on 30 September 1997.

strengthened in the afternoon, the temperature starts to rise until 1800 UTC (local noon time), when it reaches its maximum value. After this time, the temperature decreases again. This pattern of the temporal variation in surface temperature is expected. It is typical for dry land types with low soil moisture, because the substance that comprises the land surface has low heat capacity. For this reason, surface temperature responds quickly to the change in solar radiation input. For the present case, temperatures rise about 20 K within a 6-h period. In regard to the spatial variation, the northern sites in general exhibit lower temperatures than the southern sites. For any given time, temperature varies by about 5–~10 K from site to site. The relatively large magnitude of spatial and temporal variations in land surface temperatures, as compared to the smaller variation of sea surface temperatures, makes it difficult for an accurate determination and validation of LST from satellites.

Based on the temporal variation of temperatures shown in figure 2, we selected the surface temperature values collocated and coincident with the satellite overpass. For the present case, NOAA-12 passed the CF at 0018 UTC. Because polar orbiting satellites generally take about 100 min to make a complete loop around the Earth, it was estimated that it would take NOAA-12 about 2 min to pass through the ARM-SGP's satellite retrieval domain. Thus, the overpass time for the EF sites would differ from that for the CF by less than 1 min. We used a latitude–longitude map of the satellite retrieval domain to locate the pixel index for each external site, as well as the retrieved LSTs from the two algorithms. The collocated and coincident LSTs determined from surface measurements at the eight sites and satellite retrievals were subsequently compared and error statistics computed. For the atmospheric correction algorithm, the mean and rms errors are 0.56 K and 2.13 K, respectively.

Validations of the retrieved LST based on the atmospheric correction method using available SIROS and SIRS data at CF and EF sites were also carried out for all the cases listed in tables 1 and 2. Figures 3 and 4 compare the retrieved LSTs with the collocated and coincident observed surface temperatures derived from SIROS and SIRS data, respectively. Each point on the diagonal line signifies that the retrieved value is equal to the observed value. There are a total of 94 pairs of retrieved–observed LST comparisons in figure 3 and 22 pairs in figure 4. Figure 3 includes comparisons of LSTs based on the atmospheric correction method at various EF sites, where the mean and rms differences are −0.66 and 2.53 K, respectively. Figure 4 contains comparisons of LSTs based on both algorithms at the CF site only, where the mean and rms differences are 0.73 and 2.46 K for the atmospheric correction method, and 1.59 and 2.59 K for the split-window method. Brutsaert *et al.* (1993) noted that to achieve acceptable accuracies in the flux calculations, it appears that the temperature measurements should have errors smaller than 0.5 K. We found that in the present study, the accuracy of the atmospheric correction method is closer to the surface flux calculation requirement than the split-window method.

Figure 5 illustrates the dependence of LST errors produced using the atmospheric correction algorithm on the distance from the CF. For each scene, the retrieved LST is based on the transmittances and atmospheric radiances computed from the sounding profiles at the CF. Thus, errors in LST are expected to increase with increasing distance from the CF. Figure 5 shows that the mean and rms errors are 0.46 K and 1.53 K, respectively, over the CF. For the distance between 0 and 150 km, the magnitude of both the mean and rms errors increases to −1.05 and 2.45 K. Beyond 100 km, the magnitude of error stays about the same, and there is no obvious relationship between the error magnitude and the distance from the CF site. In short,

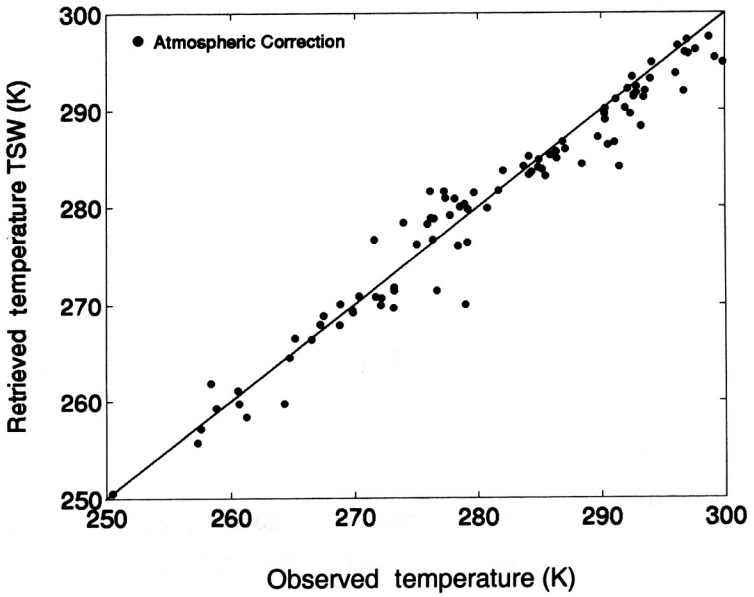

Figure 3. Comparison of the LSTs retrieved from the atmospheric correction method with collocated and coincident surface observed temperatures derived from the SIROS data at 14 External Facility sites for 94 cases in 1997. The mean and rms differences are −0.66 and 2.53 K, respectively.

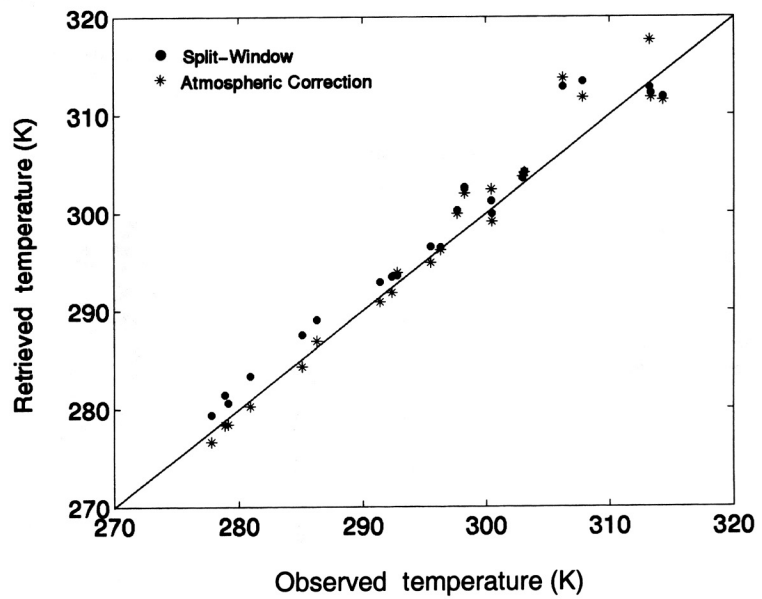

Figure 4. Comparison of the LSTs retrieved from both the atmospheric correction and the split-window methods with collocated and coincident surface observed temperatures derived from the SIRS data at the Central Facility for 22 cases in 1999. For the atmospheric correction method, the mean and rms errors are 0.73 and 2.46 K, respectively. For the split-window method, the mean and rms errors are 1.59 and 2.59 K, respectively.

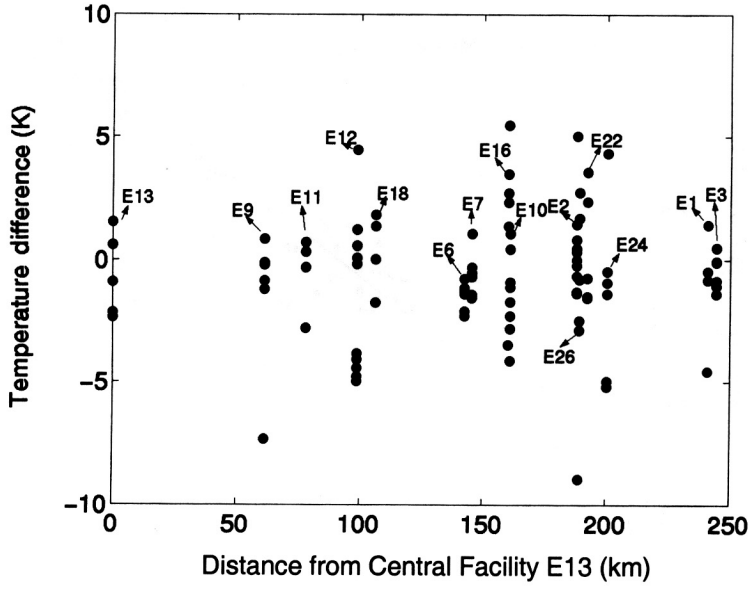

Figure 5. Sensitivity of errors in LSTs retrieved from the atmospheric correction algorithm for 1997 cases to the distance from the Central Facility.

figure 5 implies that it is necessary to obtain accurate sounding profiles to achieve high accuracy for the LST retrievals based on the atmospheric correction method. In practice, it is suggested that the distance between the retrieved pixel and the sounding launch site be no more than 150 km.

Figure 6 shows the dependence of LST errors from the atmospheric correction

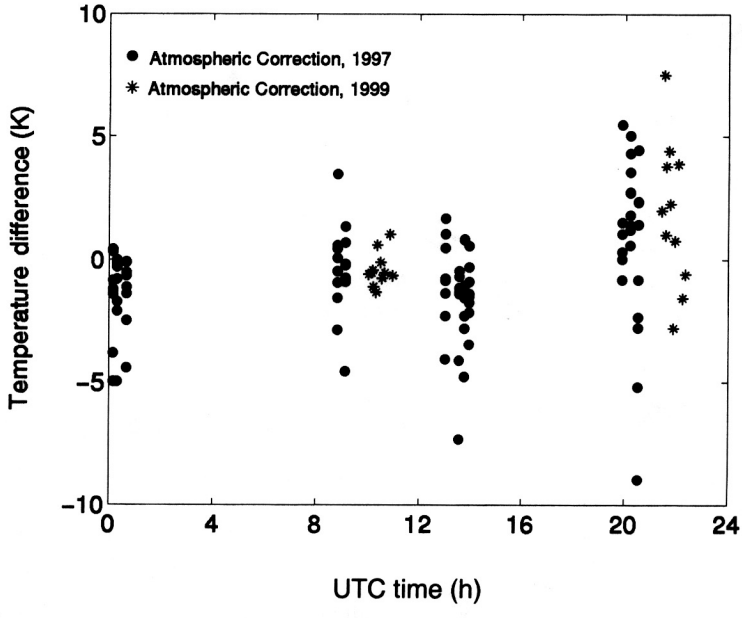

Figure 6. Sensitivity of errors in LSTs retrieved from the atmospheric correction algorithm for both 1997 and 1999 cases on the UTC time of the day.

algorithm on the UTC time of day. These data are grouped in terms of six satellite overpass times (0000 and 1300 UTC for NOAA-12, and 0900, 1000, 2000 and 2200 UTC for NOAA-14). The magnitude of error at local night-time (~0900 and 1000 UTC) is generally smaller than that at local daytime (~2000 and 2200 UTC) for both NOAA-12 and NOAA-14 overpasses. A similar pattern is also evident in figure 4, where the retrieved LSTs are closer to the values observed during local night-time (smaller LST) than those observed during local daytime (larger LST). This is due to the fact that the surface temperatures are lower and more uniform during night-time than daytime. Because of the inhomogeneity of surface properties, the discontinuity between the surface-air and surface temperatures, and perhaps the *shadowing* effects, the spread of daytime LSTs tends to be larger and, therefore, the retrieval of LST appears to be more difficult with greater uncertainties. In addition, errors for the 1999 dataset, which were collected over the CF only, are generally smaller than errors for the 1997 cases at both local night-time and daytime. This is because errors for the 1997 cases are caused by uncertainties in the sounding profiles, surface inhomogeneity and the diurnal variation, while the errors for the 1999 cases depend on surface inhomogeneity and diurnal variation only. Thus, to achieve high accuracy in LST retrievals, we need not only to employ accurate sounding profiles, but also to characterize the radiative effects of surface inhomogeneity in more detail and to improve the daytime retrievals by using auxiliary information such as the visible channel reflectance.

5. Conclusions

In this paper, we examined the difference in the performance of the atmospheric correction and split-window algorithms, and compared the retrieved LSTs with collocated and coincident surface observations. We acquired AVHRR data, ground-based surface temperature measurements, and balloon-borne atmospheric sounding profiles over the ARM-SGP CART site for a number of selected clear and mostly clear dates. The MODTRAN 3.7 code was used to compute atmospheric transmittances and radiances.

We first illustrated the results derived from a single case involving the NOAA-14 overpass at 1023 UTC on 13 October 1999. At the time of the satellite overpass, the CART site was completely cloudless, as shown in the 10.9 μm brightness temperature image. The 10.9 μm brightness temperature image also shows some of the terrain features, including rivers, metropolitan areas, etc. The retrieved LSTs from the split-window algorithm were on average 3 K higher than those from the atmospheric correction algorithm, possibly due to the uncertainty in the correction of water vapour emission/absorption effects. We then compared the retrieved LSTs with the collocated and coincident observed surface temperatures derived from SIROS and SIRS data. The error magnitudes produced from the atmospheric correction method were generally smaller than those from the split-window scheme. Comparison of the retrieved LSTs with surface observations obtained from the Central and EF sites over the SGP area showed that the mean and rms errors of the retrieved LSTs from the atmospheric correction scheme were smaller than those from the split-window scheme. Finally, we demonstrated that the atmospheric correction method is most effective for application to satellite pixels less than 150 km away from the balloon sounding launch site, and that the retrieval accuracy is better during night-time than daytime.

Acknowledgments

This work has been supported, in part, by the National Aeronautics and Space Administration (grant NAG8-1518) and by the National Science Foundation (grant ATM-9708622). Data were obtained from the Atmospheric Radiation Measurement (ARM) Program sponsored by the US Department of Energy, Office of Science, Office of Biological and Environmental Research, Environmental Sciences Division. P. Minnet provided technical assistance in decoding the satellite data. P. Rolland provided the software for reading the satellite data. N. Larsen, formerly at Raytheon, kindly supplied IDL routines for the display of satellite data and retrieval results. Preliminary processing of the satellite data was carried out by R. Hansell.

References

BECKER, F., and LI, Z., 1990, Toward a local split-window method over land surface. *International Journal of Remote Sensing*, **11**, 369–393.

BECKER, F., and LI, Z.-L., 1995, Surface temperature and emissivity at various scales: definition, measurement and related problems. *Remote Sensing Review*, **12**, 225–253.

BERK, A., BERNSTEIN, L. S., and ROBERTSON, D. C., 1989, MODTRAN: a moderate resolution model for LOWTRAN 7. Report AFGL-TR-89-0122, Air Force Geophysics Laboratory, Hanscom, AFB, MA 01731, USA.

BRUTSAERT, W., HSU, A. Y., and SCHMUGGE, T. J., 1993, Parameterization of surface heat fluxes above forest with satellite thermal sensing and boundary layer soundings. *Journal of Applied Meteorology*, **32**, 909–917.

COLL, C., and CASELLES, V., 1997, A global split-window algorithm for land surface temperature from AVHRR data: validation and algorithm comparison. *Journal of Geophysical Research*, **102**, 16 697–16 713.

DOZIER, J., and WAN, Z., 1994, Development of practical multiband algorithms for estimating land-surface temperature from EOS/MODIS data. *Advances in Space Research*, **13**, 81–90.

KNEIZYS, F. X., SHETTLE, E. P., GALLERY, W. O., CHETWYND, J. H., ABREU, L. W., SELBY, J. E. A., CLOUGH, S. A., and FENN, R. W., 1983, Atmospheric transmittance/radiance: computer code LOWTRAN 6. Report AFGL-TR-83-0187 (NTIS AD A137796). Hanscom AFB, Bedford, MA, USA.

KNEIZYS, F. X., SHETTLE, E. P., ABREU, L. W., ANDERSON G. P., CHETWYND, J. H., GALLERY, W. O., SELBY, J. E. A., and CLOUGH, S. A., 1988, Atmospheric transmittance/radiance: the LOWTRAN 7 model. Report AFGL-TR-88-0177. Hanscom AFB, Bedford, MA, USA.

LIOU, K. N., 1992, *Radiation and Cloud Processes in the Atmosphere. Theory, Observation and Modeling* (New York: Oxford University Press), 487 pp.

PRATA, A. J., 1994, Land surface temperatures derived from the Advanced Very High Resolution Radiometer and the Along Track Scanning Radiometer. II Experimental results and validation of AVHRR algorithms. *Journal of Geophysical Research*, **99**, 13 025–13 058.

SUTHERLAND, R. A., 1986, Broadband and spectral emissivities (2–18 μm) of some natural soils and vegetation. *J. Atmos. Oceanic Tech.*, **3**, 199–202.

WAN, Z., and DOZIER, J., 1996, A generalized split-window algorithm for retrieving land-surface temperature from space. *IEEE Transactions on Geosciences and Remote Sensing*, **34**, 892–905.